A common origin for cosmic explosions inferred from calorimetry of GRB030329

ARTICLE *in* NATURE · DECEMBER 2003

Impact Factor: 41.46 · DOI: 10.1038/nature01998 · Source: arXiv

11 AUTHORS, INCLUDING:

Guy G. Pooley
University of Cambridge
270 PUBLICATIONS **4,975** CITATIONS
SEE PROFILE

Derek B. Fox
Pennsylvania State University
579 PUBLICATIONS **9,051** CITATIONS
SEE PROFILE

A common origin for cosmic explosions inferred from calorimetry of GRB030329

E. Berger[1], S. R. Kulkarni[1], G. Pooley[4], D. A. Frail[5], V. McIntyre[6], R. M. Wark[7], R. Sari[2], A. M. Soderberg[1], D. W. Fox[1], S. Yost[3] & P. A. Price[8]

[1]*Caltech Optical Observatories 105-24,* [2]*Theoretical Astrophysics 130-33,* [3]*Space Radiation Laboratory 220-47, California Institute of Technology, Pasadena, California 91125, USA*
[4]*Mullard Radio Astronomy Observatory, Cavendish Laboratory, Madingley Road, Cambridge CB3 0HE, UK*
[5]*National Radio Astronomy Observatory, P O Box 0, Socorro, New Mexico 87801, USA*
[6]*Australia Telescope National Facility, CSIRO, P O Box 76, Epping, New South Wales 1710, Australia*
[7]*Australia Telescope National Facility, CSRIO, Locked Bag 194, Narrabri, New South Wales 2390 Australia*
[8]*RSAA, ANU, Mt Stromlo Observatory, via Cotter Rd, Weston Creek, Australian Capital Territory, 2611, Australia*

Past studies[1–3] have suggested that long-duration γ-ray bursts have a 'standard' energy of $E_\gamma \approx 10^{51}$ erg in the ultra-relativistic ejecta, after correcting for asymmetries in the explosion ('jets'). But a group of sub-energetic bursts, including the peculiar GRB980425 associated[4] with the supernova SN1998bw ($E_\gamma \approx 10^{48}$ erg), has recently been identified[2,3]. Here we report radio observations of GRB030329 that allow us to undertake calorimetry of the explosion. Our data require a two-component explosion: a narrow (5° opening angle) ultra-relativistic component responsible for the γ-rays and early afterglow, and a wide, mildly relativistic component that produces the radio and optical afterglow more than 1.5 days after the explosion. The total energy release, which is dominated by the wide component, is similar[1–3,5] to that of other γ-ray bursts, but the contribution of the γ-rays is energetically minor. Given the firm link[6,7] of GRB030329 with SN2003dh, our result indicates a common origin for cosmic explosions in which, for reasons not yet understood, the energy in the highest-velocity ejecta is extremely variable.

We initiated observations of the nearby GRB030329 (redshift $z = 0.1685$) in the centimetre band approximately 13.8 h after the burst. The log of the observations and the resulting light curves are displayed in Tables 1 and 2 and Fig. 1. The afterglow was also observed extensively in the millimetre (100 GHz) and submillimetre (250 GHz) bands[8]. Although this is the brightest radio afterglow detected to date, the low redshift results in a peak luminosity, $L_{\nu,\mathrm{p}}(8.5\,\mathrm{GHz}) \approx 1.8 \times 10^{31}\,\mathrm{erg\,s^{-1}\,Hz^{-1}}$, typical[9] of other long-duration γ-ray bursts (GRBs).

The observed rapid decline, $F_\nu \propto t^{-1.9}$ at $t \gtrsim 10$ d and the decrease in peak flux at $\nu \lesssim 22.5$ GHz (Fig. 1) are the hallmarks of a collimated explosion. In this framework[10], the sharp decline (or 'jet break') occurs at the time, t_j, when $\Gamma(t_j) \approx \theta_\mathrm{j}^{-1}$ owing to relativistic aberration ('beaming') and rapid sideways expansion; here Γ is the bulk Lorentz factor and θ_j is the opening angle of the jet. We model the afterglow emission (compare refs 5, 11) from 4.9 to 250 GHz assuming a uniform[10] as well as a "wind"[12] (particle density profile, $\rho \propto r^{-2}$, where r is the distance from the source) circumburst medium. Neither model is strongly preferred, but $t_\mathrm{j,rad} \approx 9.8$ d is required (Fig. 1).

Using the inferred particle density of $n \approx 1.8\,\mathrm{cm^{-3}}$ and assuming a γ-ray efficiency, $\epsilon_\gamma = 0.2$ (see ref. 3) we infer $\theta_\mathrm{j,rad} \approx 0.3$ rad, or 17°. The kinetic energy in the explosion corrected for collimation is $E_\mathrm{K} = f_\mathrm{b} E_\mathrm{K,iso} \approx 2.5 \times 10^{50}$ erg, where $f_\mathrm{b} = [1 - \cos(\theta_\mathrm{j})]$ is the beaming fraction and $E_\mathrm{K,iso}$ is the isotropic equivalent kinetic energy. This value is comparable to that inferred from modelling of other afterglows[5].

In contrast to the above discussion, Price *et al.*[13] note a sharp break in the optical afterglow at $t = 0.55$ d (Fig. 2). The X-ray flux[14] tracks the optical afterglow for the first day, with a break consistent with that seen in the optical. Thus the break at 0.55 d is not due to a change in the ambient density as, for typical parameters[15,16], the X-ray emission is not sensitive to density. However, unlike the optical emission, the X-ray flux at later times continues to decrease monotonically. Thus, we conclude that there are two emitting components: one responsible for the early optical and X-ray emission, and the other responsible for the optical emission beyond 1.5 d.

The first component, given the characteristic t^{-2} decay for both the X-ray and optical emission, is reasonably modelled by a jet. For the parameters used above (n, ϵ_γ), the opening angle is 0.09 rad or 5°.

The resurgence in the optical emission at 1.5 d requires a second component. An increase in the ambient density cannot explain this resurgence as the predicted decrease in radio luminosity, arising from the increase in synchrotron self-absorption, is not observed (Fig 1). An increase in the energy of the first component, for example by successive shells with lower Lorentz factors as advocated by Granot *et al.*[17], is ruled out by the lack[8] of strong radio or millimetric emission expected[18] from reverse shocks.

Thus, by a process of elimination, we are led to a two-component explosion model in which the first component (a narrow jet, 5°)

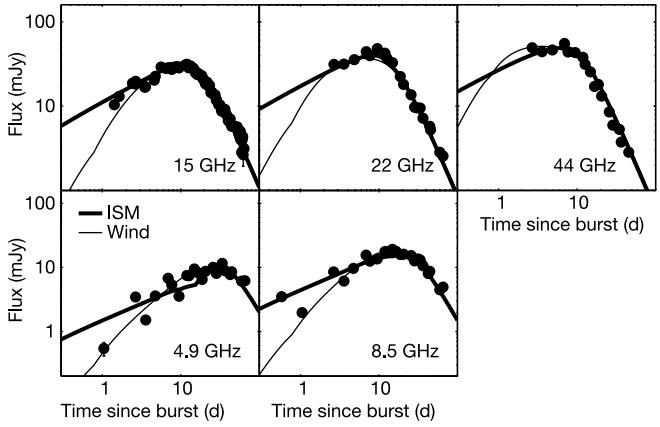

Figure 1 Radio light curves of the afterglow of GRB030329. All measurements include 1σ error bars, which in most cases are smaller than the symbols. The data are summarized in Tables 1 and 2. The solid lines are models of synchrotron emission from collimated relativistic ejecta expanding into uniform[10] (thick) and wind[12] $\rho \propto r^{-2}$ (thin) circumburst media; these models include the millimetre and submillimetre data[8]. We find $\chi^2_r = 31.3$ and 39.8 (164 degrees of freedom) for the uniform density and wind models, respectively; these include a 2% systematic error added in quadrature to each measurement. The large values of χ^2_r are dominated by interstellar scintillation (ISS) at $\nu \lesssim 15$ GHz and mild deviations from the expected smooth behaviour at the high frequencies. Comparing the data and models, we find r.m.s. flux modulations of 0.25 at 4.9 GHz, 0.15 at 8.5 GHz, and 0.08 at 15 GHz, as well as a drop by a factor of three in the level of modulation from ~3 to 40 d. These properties are expected in weak ISS as the fireball expands on the sky. The inferred source size of about 20 μas (that is, $\sim 2 \times 10^{17}$ cm) at $t \approx 15$ d is in close agreement with theoretical expectations[22]. In the uniform density model the jet break occurs at $t \approx 10$ d corresponding to an opening angle, $\theta_\mathrm{j} \approx 0.3$ (17°). From the derived synchrotron parameters (at $t = t_\mathrm{j}$: self-absorption frequency $\nu_\mathrm{a} \approx 19$ GHz, synchrotron characteristic frequency $\nu_\mathrm{m} \approx 43$ GHz, synchrotron peak flux $F_{\nu,\mathrm{m}} \approx 96$ mJy) we find an isotropic kinetic energy, $E_\mathrm{K,iso} \approx 5.6 \times 10^{51} \nu_{\mathrm{c},13}^{1/4}$ erg, a circumburst density $n = 1.8 \nu_{\mathrm{c},13}^{3/4}\,\mathrm{cm^{-3}}$, and the fractions of energy in the relativistic electrons and magnetic field of $0.16\nu_{\mathrm{c},13}^{1/4}$ and $0.10\nu_{\mathrm{c},13}^{-5/4}$, respectively; here $\nu_\mathrm{c} = 10^{13}\nu_{\mathrm{c},13}$ is the synchrotron cooling frequency, and a constraint on inverse Compton cooling as advocated by ref. 23 indicates $\nu_{\mathrm{c},13} \lesssim 1$. The beaming-corrected kinetic energy is $E_\mathrm{K} \approx 2.5 \times 10^{50} \nu_{\mathrm{c},13}^{1/4}$ erg, typical of other well-studied long-duration GRBs[5]. The parameters derived from the wind model are consistent with those from the uniform density model to within 10%.

Table 1 **Radio observations made with the VLA and the ATCA**

Epoch (UT)	Δt (d)	$F_{1.43}$ (mJy)	$F_{4.86}$ (mJy)	$F_{8.46}$ (mJy)	$F_{15.0}$ (mJy)	$F_{22.5}$ (mJy)	$F_{43.3}$ (mJy)
Mar.30.06	0.58	–	–	3.50 ± 0.06	–	–	–
Mar.30.53	1.05	–	0.54 ± 0.13	1.98 ± 0.17	–	–	–
Apr.1.13	2.65	< 0.21	3.45 ± 0.05	8.50 ± 0.05	19.68 ± 0.14	30.40 ± 0.06	46.63 ± 0.18
Apr.2.05	3.57	< 0.30	1.51 ± 0.05	6.11 ± 0.04	16.98 ± 0.19	31.59 ± 0.14	44.17 ± 0.35
Apr.3.21	4.76	< 0.36	3.58 ± 0.04	9.68 ± 0.03	22.59 ± 0.12	35.57 ± 0.09	46.32 ± 0.23
Apr.5.37	6.89	< 0.40	6.77 ± 0.08	15.56 ± 0.06	28.58 ± 0.20	44.09 ± 0.15	55.33 ± 0.43
Apr.6.16	7.68	< 0.25	5.34 ± 0.10	12.55 ± 0.21	27.26 ± 0.21	39.68 ± 0.20	43.81 ± 1.00
Apr.7.97	9.49	< 0.68	3.55 ± 0.11	13.58 ± 0.09	28.50 ± 0.23	48.16 ± 0.23	43.06 ± 1.33
Apr.10.38	11.90	< 0.58	7.51 ± 0.08	17.70 ± 0.05	31.40 ± 0.25	42.50 ± 0.14	37.86 ± 0.46
Apr.11.17	12.69	–	7.42 ± 0.09	17.28 ± 0.10	29.60 ± 0.29	36.84 ± 0.16	31.26 ± 0.51
Apr.13.35	14.87	–	9.49 ± 0.13	19.15 ± 0.08	26.78 ± 0.33	32.69 ± 0.13	25.44 ± 0.51
Apr.15.14	16.66	–	8.21 ± 0.08	17.77 ± 0.10	24.50 ± 0.31	–	17.10 ± 0.71
Apr.17.20	18.72	< 0.63	6.50 ± 0.11	15.92 ± 0.07	22.02 ± 0.25	22.41 ± 0.08	18.07 ± 0.28
Apr.19.06	20.58	–	8.66 ± 0.10	16.08 ± 0.06	18.35 ± 0.24	18.03 ± 0.11	13.15 ± 0.29
Apr.24.18	25.70	–	10.04 ± 0.08	15.34 ± 0.06	13.93 ± 0.26	13.63 ± 0.13	8.54 ± 0.48
Apr.26.92	28.44	< 0.58	8.05 ± 0.08	12.67 ± 0.09	11.82 ± 0.26	9.75 ± 0.23	5.95 ± 0.62
Apr.28.96	30.48	–	–	–	10.40 ± 0.33	9.53 ± 0.21	–
Apr.29.99	31.51	–	9.80 ± 0.09	13.55 ± 0.07	–	–	–
May 2.06	33.58	–	11.62 ± 0.08	13.10 ± 0.06	–	9.52 ± 0.14	–
May 3.07	34.59	–	–	–	–	–	5.30 ± 0.32
May 5.00	36.52	–	8.90 ± 0.08	10.64 ± 0.06	8.58 ± 0.17	7.20 ± 0.09	3.75 ± 0.26
May 11.03	42.55	–	7.72 ± 0.13	8.04 ± 0.08	7.03 ± 0.19	–	–
May 13.03	44.55	–	8.57 ± 0.09	8.68 ± 0.08	5.77 ± 0.22	5.75 ± 0.10	–
May 14.00	45.52	–	–	–	–	5.23 ± 0.17	2.84 ± 0.23
May 28.03	59.55	–	6.08 ± 0.10	4.48 ± 0.09	2.82 ± 0.21	2.84 ± 0.20	–
June 4.01	66.53	1.94 ± 0.06	6.20 ± 0.08	4.93 ± 0.06	–	2.56 ± 0.12	–

Observations commenced on March 30.06 UT, with a single 7-h observation with the Australia Telescope Compact Array (ATCA) on March 30.53 UT. In the initial observation we detected a point source at α(J2000) = 10 h 44 min 49.95 s, δ(J2000) = 21° 31′ 17.38″, with an uncertainty of about 0.1 arcsec in each coordinate, consistent with the position of the optical counterpart. In all Very Large Array (VLA) observations we used the standard continuum mode with 2 × 50 MHz bands. At 22.5 and 43.3 GHz we used referenced pointing scans to correct for the systematic 10–20 arcsec pointing errors of the VLA antennas. We used the extra-galactic sources 3C147 (J0542+498) and 3C286 (J1331+305) for flux calibration, while the phase was monitored using J1111+199 at 1.43 GHz and J1051+213 at all other frequencies. The ATCA observations were performed at 4.80, 6.21, 8.26 and 9.02 GHz with a bandwidth of 64 MHz in each frequency. The phase was monitored using J1049+215, while the flux was calibrated using J1934−638. The data were reduced and analysed using the Astronomical Image Processing System (VLA) and the Multichannel Image Reconstruction, Image Analysis and Display package (ATCA). The flux density and uncertainty were measured from the resulting maps by fitting a gaussian model to the afterglow. In addition to the r.m.s. noise in each measurement we estimate a systematic uncertainty of about 2% due to uncertainty in the absolute flux calibration.

with initially larger Γ is responsible for the γ-ray burst and the early optical and X-ray afterglow including the break at 0.55 d, while the second component (a wider jet, 17°) powers the radio afterglow and late optical emission (Fig 2). The break due to the second component is readily seen in the radio afterglow, but is masked by SN2003dh in the optical bands, thus requiring careful subtraction (Fig 2). Such a two-component jet finds a natural explanation in the collapsar model[19].

The beaming-corrected γ-ray energy, emitted by the narrow jet, is only $E_\gamma \approx 5 \times 10^{49}$ erg, significantly lower than the strong clustering[3] around 1.3×10^{51} erg seen in most bursts. Similarly, the beaming-corrected X-ray luminosity[14] at $t = 10$ h, a proxy for the kinetic energy of the afterglow on that timescale, is $L_{X,10} \approx 3 \times 10^{43}$ erg s^{-1}, a factor of ten below the tightly clustered values[2] for most other bursts. However, the second component, which is mildly relativistic (as determined by the lower energy peak of its spectrum), carries the bulk of the energy, as indicated by our modelling of the radio emission. We note that our model, with the energy in the lower Lorentz factor component dominating over the narrow ultra-relativistic component, is not consistent with the "universal standard jet" model[20].

The afterglow calorimetry presented here has important ramifications for our understanding of GRB engines. Recently, we have come to recognize a subclass of cosmological GRBs marked by rapidly fading afterglows at early time (that is, similar to GRB030329). These events are sub-energetic[2,3] in E_γ and early X-ray afterglow luminosity. However, as demonstrated by our calorimetry of GRB030329, such bursts may have total explosive yields similar to other GRBs (Fig 3).

This leads to the following conclusions. First, radio calorimetry,

Table 2 **Radio observations made with the Ryle Telescope at Cambridge, UK**

Epoch (UT)	Δt (d)	$F_{15.3}$ (mJy)	Epoch (UT)	Δt (d)	$F_{15.3}$ (mJy)
Mar. 30.91	1.43	10.38 ± 0.28	Apr. 21.72	23.24	17.63 ± 0.29
Mar. 31.12	1.64	13.05 ± 0.28	Apr. 22.66	24.18	14.51 ± 0.49
Mar. 31.91	2.43	18.66 ± 0.28	Apr. 23.33	24.85	14.62 ± 0.49
Apr. 1.12	2.64	18.29 ± 0.28	Apr. 25.81	27.33	13.60 ± 0.65
Apr. 1.98	3.50	16.75 ± 0.27	Apr. 26.82	28.34	11.78 ± 0.52
Apr. 3.07	4.59	20.36 ± 0.45	Apr. 29.82	31.34	10.35 ± 0.49
Apr. 4.09	5.61	29.13 ± 0.52	May 1.63	33.15	8.73 ± 0.52
Apr. 4.97	6.49	27.97 ± 0.26	May 4.80	36.32	9.15 ± 0.50
Apr. 5.97	7.49	28.69 ± 0.26	May 6.83	38.35	7.87 ± 0.50
Apr. 7.06	8.58	29.29 ± 0.49	May 8.73	40.25	6.70 ± 0.50
Apr. 7.89	9.41	29.15 ± 0.44	May 10.76	42.28	6.49 ± 0.50
Apr. 9.89	11.41	30.78 ± 0.51	May 15.76	47.28	5.74 ± 0.50
Apr. 11.05	12.57	28.52 ± 0.51	May 20.70	52.22	5.69 ± 0.53
Apr. 11.88	13.40	29.92 ± 0.44	May 22.76	54.28	4.78 ± 0.78
Apr. 13.05	14.57	27.90 ± 0.44	May 24.76	56.28	4.31 ± 0.55
Apr. 13.87	15.39	24.74 ± 0.44	May 25.56	57.08	5.04 ± 0.84
Apr. 14.82	16.34	23.60 ± 0.32	May 26.75	58.27	3.99 ± 0.63
Apr. 16.96	18.48	23.06 ± 0.24	May 28.76	60.28	3.96 ± 0.58
Apr. 17.92	19.44	20.51 ± 0.24	May 29.82	61.34	4.35 ± 0.50
Apr. 19.95	21.47	19.27 ± 0.38	May 30.76	62.28	2.65 ± 0.72
Apr. 20.72	22.24	17.53 ± 0.33	June 2.54	64.06	3.13 ± 0.76

All observations were made at 15.3 GHz by interleaving 15-min scans of GRB030329 with 2.5-min scans of the phase calibrator J1051+2119. The absolute flux scale was calibrated using 3C48 and 3C286. We used five antennas providing ten baselines in the range 35–140 m. As the position of the source is well known, the in-phase component of the vector sum of the ten base lines was used as an unbiased estimate of the flux density. The typical r.m.s. fluctuation on the signal in a 32-s integration period is 6 mJy. We also add a systematic uncertainty of ~2% due to uncertainty in the absolute flux calibration.

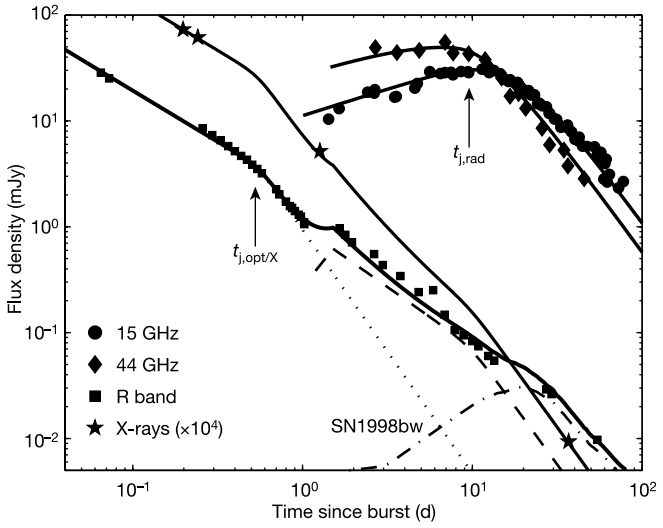

Figure 2 Radio to X-ray light curves of the afterglow of GRB030329. The optical data, from Price *et al.*[13] and the GRB Coordinates Network[24–26], have been corrected for Galactic extinction, $A_R = 0.067$ mag; we note that the latter are preliminary data. The dotted line is the model proposed by Price *et al.*[13] for the early optical emission, with $t_{j,opt} \approx 0.55$ d. The dashed line is an extrapolation of the uniform density model presented in Fig. 1 to the optical *R*-band with $\nu_{c,13} = 2$; this value is somewhat larger than the rough limit discussed in Fig. 1 legend but may be consistent with the uncertainty in the model parameters. The model in the X-ray band is based on the measured[14] optical to X-ray spectral slope and an extrapolation of the uniform density model presented in Fig. 1. The sharp increase in the optical flux at $t \lesssim 1.5$ d is due to the deceleration of the slower second jet component. Finally, the dot-dashed line is the optical emission from SN1998bw at the redshift of GRB030329, $z = 0.1685$, used as a proxy for SN2003dh[6]. The solid line in the *R*-band is a combination of the supernova and the two jet components, whereas in the radio and millimetre bands it is the uniform density model presented in Fig. 1. In the X-ray band the model is dominated by the narrow jet component. Although this two-component jet model provides a reasonable fit to the data, there are still some discrepancies which could be resolved by accurate photometry and a more careful subtraction of SN2003dh. The latter would also allow a more precise determination of the putative second jet break in the optical band at $t_{j,rad}$.

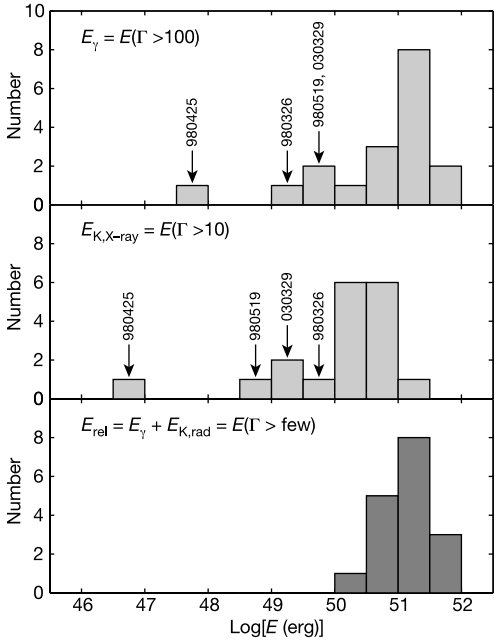

Figure 3 Histograms of various energies measured for GRBs. We plot the beaming-corrected γ-ray energy[3], E_γ, the kinetic energy inferred from X-rays at $t = 10$ h (ref. 2), $E_{K,X}$, and total relativistic energy, $E_{rel} = E_\gamma + E_K$, where E_K is the beaming-corrected kinetic energy inferred[5,21] from the broad-band afterglow. The energy in X-rays, $E_{K,X} = L_X t/\epsilon_e(\alpha_X - 1)$, with $t = 10$ h, $\epsilon_e = 0.1$, and $\alpha_X = 1.3$ is the median decay rate in the X-ray band. For GRB980519 we find that the evolution of the radio emission requires a much wider jet, $\theta_j \approx 0.3$, than what is inferred from the optical, $\theta_j \approx 0.05$; here we assume $z = 1$. We therefore infer $E_K \approx 2 \times 10^{50}$ erg from the radio data compared to $E_\gamma \approx 4 \times 10^{49}$ erg. The γ-ray energy of GRB980425 is an upper limit as the degree of collimation is not known. For the kinetic energy we use the value derived by Li and Chevalier[21] on the basis of the radio evolution of SN1998bw. There is a significantly wider dispersion E_γ and $E_{K,X}$ as compared to the total explosive yield. This indicates that engines in cosmic explosions produce approximately the same quantity of energy, thus pointing to a common origin, but the quality of these engines, as indicated by ultra-relativistic output, varies widely.

which is sensitive to all ejecta with Γ in excess of a few times unity, shows that the explosive yield of the nearest 'classical' event, GRB030329, is dominated by mildly relativistic ejecta. Ultra-relativistic ejecta, which produced the γ-ray emission, are energetically unimportant. Second, the total energy yield of GRB030329 is similar to those estimated for other bursts. Along these lines, the enigmatic GRB980425 associated[4] with the nearby supernova SN1998bw also has negligible γ-ray emission, $E_{\gamma,iso} \approx 8 \times 10^{47}$ erg; however, radio calorimetry[21] shows that even this extreme event had a similar explosive energy yield (Fig. 3). The newly recognized class of cosmic explosions, the X-ray flashes (J. Heire, J.J.M. in't Zand and S.R.K., manuscript in preparation), exhibit little or no γ-ray emission but appear to have comparable X-ray and radio afterglows to those of GRBs. Thus, the commonality of the total energy yield indicates a common origin, but apparently the ultra-relativistic output is highly variable. Unravelling what physical parameter is responsible for the variation in the 'purity' (ultra-relativistic output) of the engine appears to be the next frontier in the field of cosmic explosions. □

Received 6 June; accepted 14 August 2003; doi:10.1038/nature01998.

1. Frail, D. A. *et al.* Beaming in gamma-ray bursts: Evidence for a standard energy reservoir. *Astrophys. J.* **562,** L55–L58 (2001).
2. Berger, E., Kulkarni, S. R. & Frail, D. A. A standard kinetic energy reservoir in gamma-ray burst afterglows. *Astrophys. J.* **590,** 379–385 (2003).
3. Bloom, J. S., Frail, D. A., Kulkarni, S. R. GRB energetics and the GRB Hubble diagram: Promises and limitations. *Astrophys. J.* **594,** 674–683 (2003).
4. Galama, T. J. *et al.* An unusual supernova in the error box of the gamma-ray burst of 25 April 1998. *Nature* **395,** 670–672 (1998).
5. Panaitescu, A. & Kumar, P. Properties of relativistic jets in gamma-ray burst afterglows. *Astrophys. J.* **571,** 779–789 (2002).
6. Stanek, K. Z. *et al.* Spectroscopic discovery of the supernova 2003dh associated with GRB 030329. *Astrophys. J.* **591,** L17–L20 (2003).
7. Hjorth, J. *et al.* A very energetic supernova associated with the γ-ray burst of 29 March 2003. *Nature* **423,** 847–850 (2003).
8. Sheth, K. *et al.* GRB 030329 at millimeter wavelengths: OVRO, BIMA, & MAMBO observations. *Astrophys. J.* (submitted).
9. Frail, D. A., Kulkarni, S. R., Berger, E. & Wieringa, M. H. A complete catalog of radio afterglows: The first five years. *Astron. J.* **125,** 2299–2306 (2003).
10. Sari, R., Piran, T. & Halpern, J. P. Jets in gamma-ray bursts. *Astrophys. J.* **519,** L17–L20 (1999).
11. Berger, E. *et al.* A jet model for the afterglow emission from GRB 000301C. *Astrophys. J.* **545,** 56–62 (2000).
12. Chevalier, R. A. & Li, Z. Wind interaction models for gamma-ray burst afterglows: The case for two types of progenitors. *Astrophys. J.* **536,** 195–212 (2000).
13. Price, P. A. *et al.* The bright optical afterglow of the nearby γ-ray burst of 29 March 2003. *Nature* **423,** 844–847 (2003).
14. Tiengo, A. *et al.* The X-ray afterglow of GRB030329. Preprint at ⟨http://arXiv.org/astro-ph/0305564⟩ (2003).
15. Kumar, P. The distribution of burst energy and shock parameters for gamma-ray bursts. *Astrophys. J.* **538,** L125–L128 (2000).
16. Freedman, D. L. & Waxman, E. On the energy of gamma-ray bursts. *Astrophys. J.* **547,** 922–928 (2001).
17. Granot, J., Nakar, E., Piran, T. The variable light curve of GRB 030329. The case for refreshed shocks. Preprint at ⟨http://arXiv.org/astro-ph/0304563⟩ (2003).
18. Sari, R. & Mészáros, P. Impulsive and varying injection in gamma-ray burst afterglows. *Astrophys. J.* **535,** L33–L37 (2000).
19. MacFadyen, A. I., Woosley, S. E. & Heger, A. Supernovae, jets, and collapsars. *Astrophys. J.* **550,** 410–425 (2001).
20. Rossi, E., Lazzati, D. & Rees, M. J. Afterglow light curves, viewing angle and the jet structure of γ-ray bursts. *Mon. Not. R. Astron. Soc.* **332,** 945–950 (2002).
21. Li, Z. & Chevalier, R. A. Radio supernova SN 1998BW and its relation to GRB 980425. *Astrophys. J.* **526,** 716–726 (1999).
22. Galama, T. J. *et al.* Continued radio monitoring of the gamma-ray burst 991208. *Astrophys. J.* **585,** 899–907 (2003).
23. Sari, R. & Esin, A. A. On the synchrotron self-Compton emission from relativistic shocks and its

implications for gamma-ray burst afterglows. *Astrophys. J.* **548,** 787–799.
24. Henden, A., Canzian, B., Zeh, A. & Klose, S. GRB 030329: light curve flattens. *GRB Circ. Netw.* 2123 (2003).
25. Ibrahimov, M. A. *et al.* GRB 030329: BVRI photometry. *GRB Circ. Netw.* 2191 (2003).
26. Testa, V. *et al.* GRB 030329: VR photometry at TNG. *GRB Circ. Netw.* 2141 (2003).

Acknowledgements GRB research at Caltech is supported in part by NSF and NASA. We are indebted to S. Barthelmy and the GCN. The VLA is operated by the National Radio Astronomy Observatory, a facility of the National Science Foundation operated under cooperative agreement by Associated Universities, Inc. The Australia Telescope is funded by the Commonwealth of Australia for operations as a National Facility managed by CSIRO. The Ryle Telescope is supported by PPARC.

Competing interests statement The authors declare that they have no competing interests.

Correspondence and requests for materials should be addressed to E.B (ejb@astro.caltech.edu).

Evolution of the polarization of the optical afterglow of the γ-ray burst GRB030329

Jochen Greiner[1], Sylvio Klose[2], Klaus Reinsch[3], Hans Martin Schmid[4], Re'em Sari[5], Dieter H. Hartmann[6], Chryssa Kouveliotou[7], Arne Rau[1], Eliana Palazzi[8], Christian Straubmeier[9], Bringfried Stecklum[2], Sergej Zharikov[10], Gaghik Tovmassian[10], Otto Bärnbantner[11], Christoph Ries[11], Emmanuel Jehin[12], Arne Henden[13], Anlaug A. Kaas[14], Tommy Grav[15], Jens Hjorth[16], Holger Pedersen[16], Ralph A. M. J. Wijers[17], Andreas Kaufer[12], Hye-Sook Park[18], Grant Williams[19] & Olaf Reimer[20]

[1]*Max-Planck-Institut für extraterrestrische Physik, 85741 Garching, Germany*
[2]*Thüringer Landessternwarte Tautenburg, 07778 Tautenburg, Germany*
[3]*Universitäts-Sternwarte Göttingen, 37083 Göttingen, Germany*
[4]*Institut für Astronomie, ETH Zürich, 8092 Zürich, Switzerland*
[5]*California Institute of Technology, Theoretical Astrophysics 130-33, Pasadena, California 91125, USA*
[6]*Clemson University, Department of Physics and Astronomy, Clemson, South Carolina 29634, USA*
[7]*NSSTC, SD-50, 320 Sparkman Drive, Huntsville, Alabama 35805, USA*
[8]*Istituto di Astrofisica Spaziale e Fisica Cosmica, CNR, Sezione di Bologna, 40129 Bologna, Italy*
[9]*Physikalisches Institut, Universität Köln, 50937 Köln, Germany*
[10]*Instituto de Astronomia, UNAM, 22860 Ensenada, Mexico*
[11]*Wendelstein-Observatorium, Universitätssternwarte, 81679 München, Germany*
[12]*European Southern Observatory, Alonso de Cordova 3107, Vitacura, Casilla 19001, Santiago 19, Chile*
[13]*Universities Space Research Association, US Naval Observatory, PO Box 1149, Flagstaff, Arizona 86002, USA*
[14]*Nordic Optical Telescope, 38700 Santa Cruz de La Palma, Spain*
[15]*University of Oslo, Institute for Theoretical Astrophysics, 0315 Oslo, Norway, and Harvard-Smithsonian Center for Astrophysics, Cambridge, Massachusetts 02138, USA*
[16]*Astronomical Observatory, NBIfAFG, University of Copenhagen, 2100 Copenhagen Ø, Denmark*
[17]*Astronomical Institute Anton Pannekoek, Kruislaan 403, 1098 SJ Amsterdam, The Netherlands*
[18]*Lawrence Livermore National Laboratory, University of California, PO Box 808, Livermore, California 94551, USA*
[19]*MMT Observatory, University of Arizona, Tucson, Arizona 85721, USA*
[20]*Theoretische Weltraum- und Astrophysik, Ruhr-Universität Bochum, 44780 Bochum, Germany*

The association of a supernova with GRB030329[1,2] strongly supports the 'collapsar' model[3] of γ-ray bursts, where a relativistic jet[4] forms after the progenitor star collapses. Such jets cannot be spatially resolved because γ-ray bursts lie at cosmological distances; their existence is instead inferred from 'breaks' in the light curves of the afterglows, and from the theoretical desire to reduce the estimated total energy of the burst by proposing that most of it comes out in narrow beams. Temporal evolution of the polarization of the afterglows[5–7] may provide independent evidence for the jet structure of the relativistic outflow. Small-level polarization (~1–3 per cent)[8–17] has been reported for a few bursts, but its temporal evolution has yet to be established. Here we report polarimetric observations of the afterglow of GRB030329. We establish the polarization light curve, detect sustained polarization at the per cent level, and find significant variability. The data imply that the afterglow magnetic field has a small coherence length and is mostly random, probably generated by turbulence, in contrast with the picture arising from the high polarization detected in the prompt γ-rays from GRB021206 (ref. 18).

GRB030329 triggered the High Energy Transient Explorer, HETE-II, on 29 March 2003 (11:37:14.67 UT)[19]. The discovery of the burst optical afterglow[20,21] was quickly followed by a redshift measurement[22] for the γ-ray burster of $z = 0.1685$ (~800 Mpc), thus making GRB030329 the second-closest long-duration[23] γ-ray burst ever studied, after GRB980425 (ref. 3). The proximity of GRB030329 resulted in very bright prompt and afterglow emission, leading to the best-sampled afterglow to date. Detailed optical spectroscopy revealed an underlying supernova (SN2003dh)[1,2] with an astonishing spectral similarity to SN1998bw (at

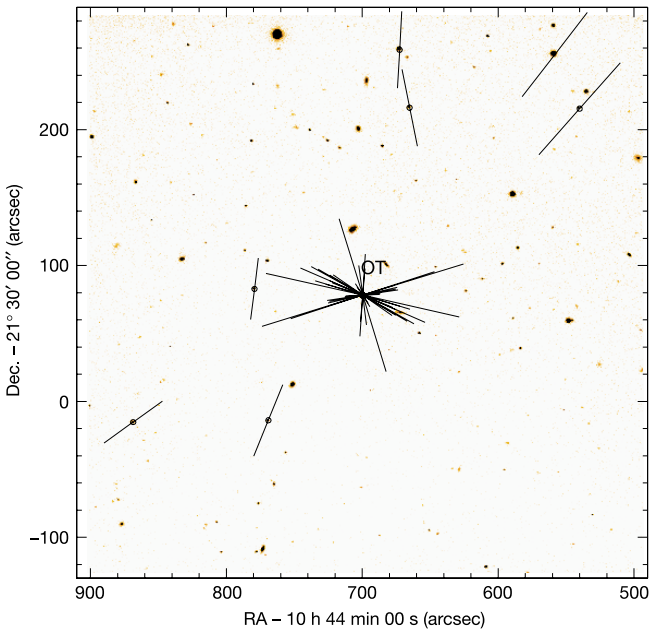

Figure 1 R band image of the field centred on the optical afterglow of GRB030329. The 27 FORS1 (Focal Reducer and Low Dispersion Spectrograph at the Very Large Telescope (VLT)/Antu) measurements are shown as 'vectors' where the length is a measure of the polarization degree, and the orientation indicates the position angle. While the afterglow varies in degree as well as angle, the polarization of seven field stars is constant within 0.1% in polarization degree and 1.5 degree in position angle throughout the 38 days. Linear polarization was measured from sets of exposures with different retarder-plate position angles. Imaging polarimetry was obtained during the first four nights (when the afterglow was brighter than 17th magnitude) from sixteen different retarder-plate angles, and from eight angles thereafter. Because the FORS1 polarization optics allows determination of the degree of polarization to an accuracy of $<3 \times 10^{-4}$ and of the polarization angle to ~0.2°, we consider the above variance of the field stars to represent the systematic error over the 38-day time period. Observations of polarimetric standard stars reproduced their tabulated values within 5%. The FORS1 retarder-plate zero-point angle of −1.2° was subtracted from the polarization angle. The position angle has a systematic uncertainty of ±1.5°, which was added in quadrature to the statistical errors. OT, optical transient.